International Journal of Sediment Research xxx (xxxx) xxx

Contents lists available at ScienceDirect

International Journal of Sediment Research

journal homepage: www.elsevier.com/locate/ijsrc

Original Research

Three-dimensional numerical modeling of sediment transport in a highly turbid estuary with pronounced seasonal variations

Thi-Kim-Anh Do [a, b, *], Nicolas Huybrechts [a, b], Isabel Jálon-Rojas [c], Pablo Tassi [d], Aldo Sottolichio [c]

[a] Cerema Risques, Eaux et Mer (CEREMA REM), RHITME Research Team, Margny-lès-Compiègne F-60280, France
[b] Université Rouen Normandie, Université Caen Normandie, CNRS, Normandie Université, M2C, UMR 6143, Margny Lès Compiègne F-60280, France
[c] Univ. Bordeaux, CNRS, Bordeaux INP, EPOC, UMR 5805, Pessac F-33600, France
[d] Electricity of France EDF R&D and Laboratoire d'Hydraulique Saint-Venant, ENPC, Institut Polytechnique de Paris, Chatou, France

ARTICLE INFO

Article history:
Received 19 April 2024
Received in revised form
12 November 2024
Accepted 15 December 2024
Available online xxx

Keywords:
Three-dimensional (3D) modeling
Sediment transport
Settling velocity
Gironde estuary
Turbidity maximum
Open TELEMAC

ABSTRACT

Simulating sediment dynamics in a large and energetic estuary system remains challenging, primarily due to the spatial and temporal complexities of the interaction between flow and sediment transport, especially for sand-mud mixtures. This study uses a three-dimensional (3D) numerical model, based on the open TELEMAC system, to investigate the dynamics of suspended sediment concentration (SSC) in the Gironde Estuary, a complex estuarine environment characterized by an estuarine turbidity maximum (ETM) and significant variations in river discharge. The main contributions of this study include addressing the challenges of coupling bed friction with sediment transport of the sand-mud mixture for feedback on bed roughness and bottom depth changes and the ability of the model to capture the migration of ETM from high to low flow. Additionally, the current study analyzes the ability of the model to capture the migration of ETM from high to low flow, and it utilizes a calibration strategy that minimizes parameters by using *in situ* data and encompassing hydro–morpho-sedimentary interactions. A sensitivity analysis was done using different settling velocity approaches and sediment classes to establish an optimal model configuration and the uncertainty associated with the reduced model parameterization is discussed. The model satisfactorily reproduces the hydrodynamic features, particularly when the hydro-sedimentary feedbacks are taken into account, the seasonal trend of SSC, spring-neap variations, and the development of a well-defined ETM. The selection of a specific formulation for the settling velocity influences the location and magnitude of ETM. The van Leussen formula not only predicts a broad movement of ETM from high to low river flow, but also predicts high turbidity for extended periods during low river flow. Conversely, two empirical formulas from Le Hir and Defontaine predicted the highest turbidity during neap tides but sediment losses during prolonged simulations. The results of this study contribute to a deeper understanding of sediment dynamics in the Gironde Estuary, providing valuable information for future estuarine modeling and management.

1. Introduction

Located at the interface between land and sea, estuaries are among the most important coastal environments, fostering a highly energetic and dynamic sediment environment. Many estuaries have locally-elevated suspended sediment concentration (SSC), known as an estuarine turbidity maximum (ETM) (Dyer, 1988; Schubel, 1968). These ETMs are the result of the complex interaction of tides, river flow, sediment dynamics, and bed evolution (Burchard & Baumert, 1998; Dyer, 1988; Geyer, 1993; Talke & Jay, 2020). According to the literature, the ETM results from the combination of tidal pumping and density effects. In macrotidal estuaries such as the Seine and the Gironde estuaries, it has been demonstrated by three-dimensional (3D) modelling that ETM can

* Corresponding author. Cerema Risques, Eaux et Mer (CEREMA REM), RHITME Research Team, Margny-lès-Compiègne F-60280, France.
E-mail address: thi-kim-anh.do@cerema.fr (T.-K.-A. Do).
Peer review under the responsibility of International Research and Training Centre on Erosion and Sedimentation.

https://doi.org/10.1016/j.ijsrc.2024.12.003

develop under the effect of tidal pumping only, without any density stratification. However, salinity gradients are necessary to maintain a stable ETM mass within the estuary by limiting seaward dispersion of fine sediment in estuaries (Brenon & Le Hir, 1999; Sottolichio et al., 2000; van Maanen & Sottolichio, 2018). Moreover, high SSC can affect estuarine waterways and coastal regions that often require human intervention, such as dredging operations.

Significant progress has been made in understanding sediment dynamics in large and energetic estuary systems, especially by the implementation of process-based models. A deeper understanding of the dynamics and characteristics of ETMs is of great interest for managing navigation channels, protecting coastal and estuarine resources, and addressing economic stakes (McSweeney et al., 2017; Zhu et al., 2021). However, realistic simulations are still challenging due to the spatial and temporal complexity of flows and sediment transport, along with the feedback loops between them. Consequently, several recent approaches to address this question have their own limitations. For example, numerical models suffer from simplified parameterization often based on empirical approaches and limited data availability (Flores et al., 2020; Hesse et al., 2019; Sottolichio et al., 2000). These limitations manifest themselves in the models' performance, which strongly depends on the calibration process, making it challenging to effectively constrain the models for long-term periods using the available data. The satellite data approach can provide long-term data with broader spatial coverage, but it often encounters challenges in extrapolating localized measurements to the entire estuary and lacks the necessary temporal resolution to capture rapid ETM dynamics (Abascal-Zorrilla et al., 2020; Normandin et al., 2019). Furthermore, satellite data and depth-averaged numerical models provide limited information on sediment fluxes throughout the water column. Continuous long-term in-situ monitoring programs offer high-frequency data (Druine et al., 2018; Fettweis et al., 2019; Jalón-Rojas et al., 2015, 2016; Matos et al., 2020) but are restricted to specific points within the estuary.

To overcome these challenges and achieve a comprehensive understanding of ETM dynamics, high-complexity numerical models represent a relevant approach to capture the overall three-dimensional variability of the system. These models can integrate various parameters and simulate complex processes, allowing for a deeper understanding of the sediment dynamics. Although three-dimensional process-based models have advanced due to improved computational resources, accurately modeling the dynamics of sediment, especially fine-grained sediment or sand-mud mixtures, remains a challenge. The behavior of mixed sediment in the near-bed region and the water column is still not fully understood (Chou et al., 2018), such as flocculation processes, hindered settling of suspensions, and consolidation of the bed (Winterwerp & van Kesteren, 2004). Compared to pure sand and pure mud, the erodibility of sand-mud mixtures remains insufficiently understood, especially when the mud material contains silt (Chen et al., 2021; Zhang et al., 2022). This knowledge gap can be particularly problematic when modeling hyperturbid energetic systems where intricate feedback loops between sediment and flow are a fundamental aspect of the system's behavior even at seasonal scales (Jalón-Rojas et al., 2018, 2021). For instance, it has been noticed that numerical models generally do not correctly capture the upstream migration of the ETM during low flow periods (Diaz et al., 2020; Lajaunie-Salla et al., 2017). This migration induces complex interaction between sediment dynamic and hydrodynamic patterns. One such interaction involves fluid mud deposits, which reduce bed friction in the upstream parts, consequently increasing tidal amplitude in the summer compared to the winter period (Jalón-Rojas et al., 2018).

In fact, modeling studies that take into account the spatio-temporal variability of bottom roughness are still rare (Huybrechts et al., 2012; Villaret et al., 2011). More recently, Zhang et al. (2023) investigated the influence of bedforms such as silt ripples on bed roughness and sediment transport in the coastal zone of the subaqueous Yellow River Delta, China, using an echo sounder, by incorporating real-time bed roughness into sediment transport modeling. Zhang et al. (2023) highlights the importance of the dynamic bed roughness data as input to sediment transport models, providing a more accurate understanding of sediment dynamics in turbid coastal regions. Furthermore, several studies (Beven & Freer, 2001; Roy & Oberkampf, 2011; van Maren & Cronin, 2016) have highlighted the issue of equifinality arising from model calibration using limited datasets. Equifinality suggests that various sets of model parameters can produce results that closely align with available data for a specific scenario. Moreover, these parameter sets may not be suitable for other distinct forcing conditions. Recently, with efforts focused on reducing model complexity for suspended sediment transport, Zhang et al. (2021, 2024) developed methods to estimate settling velocity, eddy diffusivity, and pick-up rate through the best fit of the field-measured sediment profiles and a one-dimensional analytical model, eliminating the need for empirical parameters. Therefore, the development of high-complexity models capable of accurately reproducing hydro-sedimentary dynamics under changing conditions stands as a paramount scientific challenge.

Located in Western Europe, the Gironde Estuary is an example of a complex macrotidal estuary characterized by the presence of high ETMs and sand-mud mixtures in the central part of the water body. In recent years, several two-dimensional (2D) or three-dimensional (3D) numerical models have been developed for the Gironde Estuary with different complexity levels (Diaz et al., 2020; Huybrechts et al., 2012, 2021; Orseau et al., 2021; van Maanen & Sottolichio, 2018). These models aim to predict water levels or track ETM by computing hydrodynamics, sediment transport, and salt intrusion. Such models generally rely on near-surface SSC data for calibration and validation and assume a fixed bed. This approach neglects the temporal evolution of the bed, as well as the spatio-temporal variability of both bed friction components (skin friction and friction induced by bedform) or vertical gradients of SSC.

In highly-turbid estuaries such as the Gironde, it has been proven that the bed can seasonally change from sandy to muddy; the calibration of the friction coefficient may need to integrate this seasonal variability to accurately simulate the flow (Jalón-Rojas et al., 2021). Huybrechts et al. (2021) proposed friction coefficient relations based on river flow discharge, as it is the main factor that induces the spatial migration of the fluid mud in this estuary (Jalón-Rojas et al., 2015). However, this approach, designed for 2D hydrodynamic models with spatially constant bed friction coefficients by zone, creates discontinuities in the bed friction through zone delineation (Huybrechts et al., 2021) (Fig. 4). It is, thus, not adapted for morphodynamic modeling as it may be prone to unrealistic bed evolutions.

To address the complexities of modeling cohesive sediment in the highly turbid and macrotidal Gironde Estuary, the current study presents a 3D numerical model developed using the open TELEMAC system (Hervouet, 2007) to establish an optimal simulation of hydrodynamics and sediment transport. This model is built on previous 2D models implemented by Huybrechts et al. (2012, 2021) and introduces three major novel features: (i) it couples bed friction in the hydrodynamic model with mixed sediment transport, enabling feedback on bed roughness and bed changes; (ii) it applies a calibration strategy that reduces, as much as possible, the calibrated parameters, relies on *in situ* data input, and encompasses

Please cite this article as: Do, T.-K.-A et al., Three-dimensional numerical modeling of sediment transport in a highly turbid estuary with pronounced seasonal variations, International Journal of Sediment Research, https://doi.org/10.1016/j.ijsrc.2024.12.003

hydro–morpho-sedimentary interactions; (iii) it further investigates the ability of different model configurations to capture the upstream migration of ETM. Even if this research focuses especially on the Gironde Estuary, the developed methodological approach can serve to enhance the modeling strategy in other similar turbid macrotidal estuaries for instance for the Loire, Scheldt, Thames, or Ems rivers.

Sensitivity tests are done to explore the uncertainties associated with different parameters and to identify the parameters that induce the greatest impact on SSC dynamics. Recent *in situ* data, including measurements at the surface and near the bottom, are used to improve the accuracy of the model. Through this approach, the objective is to assess uncertainties and improve the understanding of the response of sediment dynamics to different model formulations, ultimately improving the reliability of estuarine modeling. The model is then used to replicate the variability and spatial distribution of hydrodynamic conditions throughout the estuary from winter to fall, focusing on the downstream to a central part of the estuary where the ETM has been observed.

2. Study site and data set

2.1. Gironde Estuary

The Gironde Estuary is a funnel-shaped macrotidal system located on the southwest coast of France (Fig. 1(a)). It covers a total surface area of 635 km^2 and drains a watershed of approximately 81,000 km^2 (Allen et al., 1980; Fuentes-Cid et al., 2014; Jalón-Rojas et al., 2015; Savoye et al., 2012). The main estuary body extends over 75 km from the mouth to the confluence of the Garonne and Dordogne rivers. Downstream from Pauillac, the estuary has a wide section, whereas upstream the estuarine section is more rapidly decreasing with the presence of sandbanks and islands. Together with the tidal region of these two rivers, a fluvio-estuarine system is formed in which the tidal wave propagates up to 180 km from the mouth (Jouanneau & Latouche, 1981). The tide is predominantly semidiurnal, with a range of 2–5.2 m at the mouth (Jalón-Rojas et al., 2018). The propagation of the tide along the estuary leads to an amplification of tidal waves and an asymmetry in the rise and fall of the water level, with durations of 4 h and 8 h and 25 min, respectively, at 100 km from the mouth. The Dordogne River and Garonne River contribute approximately 35% and 65%, respectively, to the freshwater discharge (Sottolichio, 1999). The average combined river discharge (period of 2005–2014) of the Garonne and Dordogne rivers is approximately 680 m^3/s, with a well-defined flood season from November to May (maximum daily average values exceeding 3,000 m^3/s) and a low flow period from June to October (average daily values generally below 200 m^3/s) (Coynel et al., 2004; Jalón-Rojas et al., 2015). For example, in 2018, the total daily river discharge ranged from 133 to 5,560 m^3/s during low and high river discharge periods, respectively (Orseau et al., 2021).

Studies on sediment transport in the Gironde Estuary revealed a well-defined ETM characterized by a high SSC, mainly composed of silts and clays. SSC in surface waters exceeds 1 g/L and can reach up to 10 g/L near the bottom (Castaing & Allen, 1981; Defontaine et al., 2023; Doxaran et al., 2009; Jalón-Rojas et al., 2015; Saari et al., 2010). The primary sources of fine sediment in the estuary are the Garonne and Dordogne river watersheds, as documented by Coynel (2005) and Coynel et al. (2018). Two types of ETM have been identified in the Gironde Estuary: a relatively stable ETM, permanently observed in the middle of the estuary near Pauillac, associated with a mud-trapping zone in the main channel, and a dynamic ETM that shifts along the estuary depending on the seasonal dynamics of river flow (Allen et al., 1980; Doxaran et al., 2009; Jalón-Rojas et al., 2015; Sottolichio & Castaing, 1999). During periods of high river flow, a well-defined density gradient positions the ETM at the density node (Allen et al., 1980). In contrast, during periods of low river flow, ETM can reach the upper freshwater regions of the tidal rivers under the effect of tidal pumping. Salinity intrusion also is strongly dependent on river flow. Salinity variations are particularly noticeable in the lower part of the estuary, between Pauillac and Verdon, during high river flow and extend into the riverine areas of the Garonne and Dordogne rivers during periods of low river flow (Schmidt, 2020).

2.2. Data set

The Gironde Estuary features two continuous sensor monitoring networks. The first network consists of nine water stations managed by the Grand Port Maritime of Bordeaux (GPMB) (the red triangles in Fig. 1(a)). The second network, known as MAGEST (Marel Gironde ESTuary), is an automated continuous monitoring system (Etcheber et al., 2011; Schmidt, 2020) that measures salinity, turbidity, temperature, and dissolved oxygen at the water

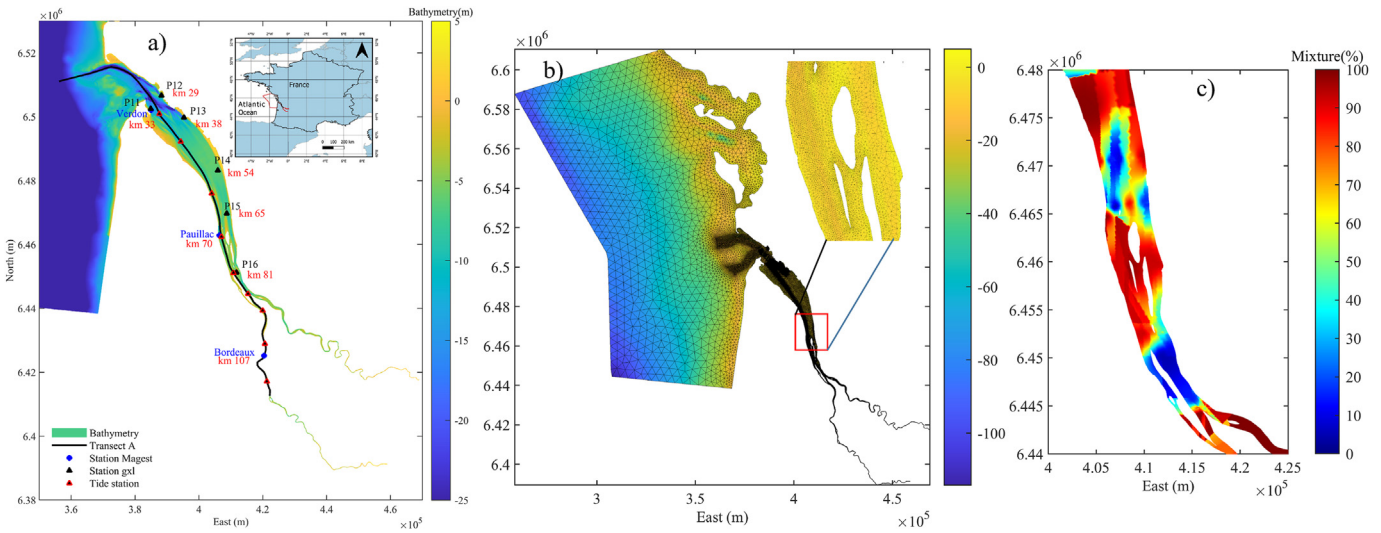

Fig. 1. Gironde Estuary including bathymetry and survey stations. (a) Location of estuary and different monitoring stations, (b) horizontal grid, and (c) mud content on the bed.

Please cite this article as: Do, T.-K.-A et al., Three-dimensional numerical modeling of sediment transport in a highly turbid estuary with pronounced seasonal variations, International Journal of Sediment Research, https://doi.org/10.1016/j.ijsrc.2024.12.003

surface at intervals of 10 min. In the main estuary body, two stations are monitored: Verdon and Pauillac (Fig. 1(a)). Although recent field surveys have been done in the estuary, they have focused primarily on specific inquiries, such as settling deposition fluxes (Defontaine et al., 2023) or circulation at the estuary mouth (Ross et al., 2019). These sparse datasets are not optimal for model calibration. Therefore, as part of the Gironde XL 3D project funded by GPMB, two surveys were done in 2018 that covered the main estuary, from the mouth to the confluence of the rivers.

The first survey was done from March to May, while the second was done from August to October at six stations (P11−P16, as shown in Fig. 1(a)). At each station, vertical velocity profiles were measured, while salinity and turbidity were recorded at the bottom every 10 min. It should be noted that during the first survey, moorings at stations P15 and P16 were reversed, leading to a lack of data collection. Therefore, the most complete dataset was obtained during the summer survey.

Furthermore, the bathymetry of the entire estuary is measured every 5 years by the Port of Bordeaux. This dataset includes bathymetric data collected for the entire estuarine section between 2010 and 2016. In addition, bimonthly surveys are done along the navigation channel. Local surveys done between mid-November 2017 and mid-January 2018 have been interpolated into the computational mesh. Bed samples also are collected annually by GPMB at several locations along the navigation channel. The data collected in December 2017 were used to estimate the initial composition of the deposited bed material in terms of the percentage of sand, coarse mud, and fine mud (as shown in Fig. 1(c)).

3. Methodology

3.1. Hydrodynamic model

In the current study, a 3D numerical model was developed using the open TELEMAC system (Hervouet, 2007). The model simulates the hydrodynamics by solving the three-dimensional Reynolds−Averaged Navier−Stokes equations on an unstructured triangular mesh that covers the entire estuary and its tributaries (hydrodynamics module TELEMAC-3D). The computational domain extends over 200 km in length and 70 km in width along the adjacent coast (Fig. 1(b)). Inland, it extends over about 180 km upstream from the estuary mouth, encompassing the upper limit of tidal influence. The horizontal grid contains 58,251 nodes and 107,562 triangular elements and has a variable resolution: fine resolution (25−30 m) around the islands and in tidal rivers, medium resolutions along the navigation channel (100 m) or in the shoals (350 m) of the estuary, and coarser resolution (4 km) offshore. The mesh has been refined along the navigation channel to ensure a minimum of five nodes across the channel width. The model uses 9 vertical sigma layers along the water column, with a finer resolution near the bottom.

Tidal harmonics, including 46 constituents, and storm surges at the open offshore boundary are used to drive the model. The tidal signal is extracted from the North East Atlantic tidal model of Pairaud et al. (2008). The salinity at the offshore boundary is set to 35 psu, while at the upstream boundary it is set to 0 psu. The daily river discharge measured for the main tributaries (the Garonne and Dordogne, https://hydro.eaufrance.fr/) is imposed at the upstream boundary. The bathymetric data of the entire estuary is interpolated onto the mesh grid. Detailed bathymetry within the navigation channel is interpolated from local surveys done in January and July 2018 to provide accurate bottom levels for the morphodynamic model. Offshore bathymetric data correspond to a digital elevation model (DEM) obtained from the Service Hydrographique et Océnographique de la Marine (SHOM). A time step of 30 s is used for all simulations. A one-month simulation with constant river flow was done to spin-up hydrodynamic and salinity conditions for the sediment transport model. The turbulence in the model is simulated using a constant diffusivity coefficient and the Prandtl mixing-length model combined with the Lehfeldt and Bloss (1988) damping functions along the horizontal and vertical directions, respectively. For bed friction, the Nikuradse (1933) formulation is selected, utilizing two different approaches to determine the bed roughness value. The first one uses a friction coefficient that is constant within each zone but varies depending on the river discharge. The calibration was done using a shallow water model (Huybrechts et al., 2021). The second approach utilizes the van Rijn (2007) bed roughness predictor, which calculates both skin roughness and bed form roughness according to the sediment size and flow properties (water depth and flow velocity).

3.2. Sediment transport model

The 3D hydrodynamic module, TELEMAC-3D, is coupled with GAIA, a module for simulating sediment transport and bed evolution processes (Tassi et al., 2023). The spatial and temporal variations of the mixed sediment consisting of sand and mud are taken into account. The transport of the sand-mud mixture will modify the median grain size and the associated value of the predicted bed roughness.

The Meyer-Peter and Müller (1948) formula (Chini & Villaret, 2007) is used to estimate the bed load of sand, while the advection-diffusion equation is solved to model the transport of cohesive material. The bed structure is discretized with 10 layers. Consolidation of mud deposits is treated using a multilayer approach, where the upper layer represents the freshest deposit and the lower layer is the most consolidated (Tassi et al., 2023). To simulate mud consolidation, mass transfer coefficients are specified for each layer and calibrated with the experimental data from Van (2012). Consequently, in the current study, the values of the mass transfer coefficient range from 1×10^{-3} to 1×10^{-6} respectively for layer 1 to layer 10 corresponding to concentration (C_{layer}) values ranging from 66 to 660 g/L.

Regarding sediment composition, two or three classes of sediment are chosen to represent the Gironde Estuary sediment that includes one class of sand (diameter (d) = 0.3 mm) and one or two classes of mud characterized by different settling velocities. The initial distribution of the sand-mud mixture (Fig. 1(c)) is based on bed samples taken near the navigation channel, with a sandy bed in the mouth and predominant mud in the central part. For the boundary conditions, the SSC values from the Naïades datasets (https://naiades.eaufrance.fr/) are imposed for the Garonne and Dordogne rivers, while a concentration equal to zero is imposed offshore.

The erosion flux, also referred as the entrainment rate, E (kg/m^2/s), is calculated using the Partheniades (1965) formula for cohesive sediment as Eq. (1):

$$E = \mathrm{E0}\left(\frac{\tau_b - \tau_{ce}}{\tau_{ce}}\right) \tag{1}$$

where E is the erosion flux, E0 is the entrainment coefficient (kg/m^2/s), τ_b is the bottom shear stress (N/m^2), and τ_{ce} is the critical shear stress for erosion (N/m^2). Bonnefille et al. (1971) demonstrated that the erosion coefficient is not constant in the Gironde Estuary. They proposed a relation between the erosion coefficient (E0) and mud concentration, valid up to 400 g/L. However, as noted by Santoro et al. (2019), imposing both a critical shear stress and an erosion coefficient that vary with mud concentration may result in an erosion flux that remains relatively constant across different

Please cite this article as: Do, T.-K.-A et al., Three-dimensional numerical modeling of sediment transport in a highly turbid estuary with pronounced seasonal variations, International Journal of Sediment Research, https://doi.org/10.1016/j.ijsrc.2024.12.003

mud concentrations, as the two effects tend to offset each other. Due to the lack of recent data covering the entire range of mud concentrations, the current study retains a constant erosion coefficient, which is consistent with previous research (Diaz et al., 2020; Lajaunie-Salla et al., 2017; van Maanen & Sottolichio, 2018).

For cohesive material, the critical shear stress for erosion depends on the consolidation state of the muddy deposit, C_{layer} (g/L). The relation between the critical shear stress, $\tau_{\text{ce,}}$ and the mud concentration, $C_{\text{layer,}}$ is calculated as Eq. (2) (GPMB, 2002):

$$\tau_{\text{ce,layer}} = \rho_{\text{m}}(0.01e^{(0.00495C_{\text{layer}}^{-0.91})})^2 \tag{2}$$

with $\rho_{\text{m}} = C_{\text{layer}} + \rho_{\text{w}}(1 - C_{\text{layer}}/\rho_{\text{s}})$ in which ρ_{w} is the water density (1,030 kg/m^3), and ρ_{s} is the sediment density (2,650 kg/m^3).

The critical shear stress for erosion ranges from 0.03 to 15 N/m^2 for, respectively, concentration (C_{layer}) values ranging from 66 to 660 g/L, respectively. For a sand-mud mixture, the erosion flux is calculated based on the mud fraction, f_{m}, i.e., the ratio between mud and the total sediment mass, following the method developed by Waeles (2005). To account for the influence of mixed sediment on bed properties, erosion rates are calculated separately for sand and mud depending on the regime type: considered as pure sand, or non-cohesive ($f_{\text{m}} < 30\%$), mud, or cohesive ($f_{\text{m}} > 50\%$), and mixed ($30\% < f_{\text{m}} < 50\%$). The calculation of the erosion flux term is implemented in GAIA, see Tassi et al. (2023) for further details.

The deposition flux, D (kg/m^2/s), is calculated from the Krone (1962) formulation for each sediment class, as the product of its specific settling velocity, w_{s} (m/s), and near-bed concentration, C_{b} (g/L), evaluated at the interface between the bedload and the suspended load (Eq. (3)):

$$D = w_{\text{s}} C_{\text{b}} \tag{3}$$

For the Gironde Estuary, different formulations of the settling velocity have been developed or used. Diaz et al. (2020) selected van Leussen (1994) formulation whereas Lajaunie-Salla et al. (2017), Le Hir et al. (2000), and van Maanen and Sottolichio (2018) used relations involving salinity and SSC. Soulsby et al. (2013) have proposed a flocculation formulation based on *in situ* measurement on several estuaries. Recently, Defontaine et al. (2023) measured the settling velocity in the upstream part of the Gironde Estuary and proposed an empirical formulation. The different formulations are reviewed in the following paragraphs and tested in this modelling study as they may impact the spatio-temporal patterns of SSC.

The van Leussen (1994) formula considers the influence of turbulence on the settling velocity accounting for flocculation processes as Eq. (4):

$$w_{\text{s}}' = w_{\text{s}}\left(\frac{1 + \text{AG}}{a + \text{BG}^2}\right) \tag{4}$$

where w'_{s} is the settling velocity depending on flocculation, and w_{s} is the settling velocity of a particular sediment class in still water. The coefficient A controls the formation of flocs by turbulence while the coefficient B controls the breaking of flocs by turbulence. The values of the coefficients are $A = 0.3$ and $B = 0.09$ corresponding to van Leussen's specifications. The value of w_{s} is prescribed as an input parameter as a known value ranging between 0.001 and 0.0005 m/s. The dissipation parameter G is used to represent the turbulence intensity and can be computed with a k–ε turbulence model.

Soulsby et al. (2013) proposed physics-based formulae based on assumptions of a two-class floc population (microflocs and macroflocs) in quasi-equilibrium with the flow. It is assumed that the settling velocities of microflocs (Eq. (5)) and macroflocs (Eq. (6)) are related to floc size and density via the Kolmogorov microscale as a function of turbulent shear–stress and sediment concentration, including height dependence and floc-density-dependence. This formulation is suitable only with one class of cohesive sediment and was chosen initially for application because it does not require calibration of the coefficients. The coefficients in the formulae were calibrated against an existing large data-set of *in situ* observations of floc size and settling velocity from Northern European estuaries (Eqs. (5) and (6)):

$$w_{s\mu} = B_{\mu}(s-1)\left(\frac{\varepsilon d_1^4}{\nu^3}\right)^{0.39} g\left(\frac{\nu}{\varepsilon}\right)^{\frac{1}{2}} \exp\left(-\left(\frac{u_{*s\mu}}{u_*\xi^{1/2}}\right)^{0.66}\right) \tag{5}$$

$$w_{\text{sM}} = B_{\text{M}}(\bar{s}_{e\mu} - 1)\left(\frac{\varepsilon \bar{d}_{\mu}^4}{\nu^3}\right)^{0.166} g c^{2.672k}\left(\frac{\nu}{\varepsilon}\right)^{1/2} \exp\left(-\left(\frac{u_{*\text{sM}}}{u_*\xi^{1/2}}\right)^{0.463}\right) \tag{6}$$

where the index M designates the macroflocs, and the index μ designates the microflocs. The term $s = \rho_{\text{s}}/\rho$ is relative effective density; ρ_{s} is the density of the primary particles's mineral component, and ρ is the water density. The variable, d_1, is the diameter of the primary paticles. $\bar{s}_{e\mu}$ is the mean relative effective density of the microfloc data, and $\bar{d}_{\mu}$ is their mean effective diameter. The values used are $s = 2.6368$, $d_1 = 10^{-5}$ m (10 μm), $\bar{s}_{e\mu} = 1.15$, and $\bar{d}_{\mu} = 10^{-4}$ m (100 μm). The concentration (c) is dimensionless and defined as c = total SSC/ρ. The parameter g (9.81 m/s^2) is the acceleration due to gravity. $B\mu$, B_{M}, $u_{*\text{sM}}$, $u_{*s\mu}$, and k are optimisable coefficients; B_{μ}, $B_{\text{M,}}$ and k are dimensionless, while $u_{*\text{sM,}}$ and $u_{*s\mu}$ have a units of m/s.

In Eqs. (5) and (6), $B_{\mu} = 0.363$, $B_{\text{M}} = 0.860$, $k = 0.825$, $u_{*\text{sM}} = 0.067$ m/s, and $u_{*s\mu} = 0.025$ m/s, which are optimized coefficients established for the Tamar and Gironde estuaries based on measured SSC. ε and ν are the turbulent kinetic energy (TKE) dissipation rate and the kinematic viscosity of the fluid. The dissipation rate (ε) can be applied directly in k–ε turbulence of the formulae in the flow/sediment model. In applications where modeled ε-profiles are not available, ε can be obtained from Eq. (7) under the assumption of steady uniform flow.

$$\varepsilon = \frac{u_*^3\xi}{Kz} \tag{7}$$

where K is von Karman's constant equal to 0.4; z is the height above the bed; u_* is the friction velocity; ξ is a dimensionless factor that describes the variation of shear stress with height, $\xi = 1 - z/h$ where h is the water depth.

Another option is to use a relation of settling velocity as a function of SSC as proposed by Le Hir et al. (2000). This formulation depends on minimum, $w_{\text{s,min}}$, and maximum, $w_{\text{s,max}}$, settling velocities for both flocculation and hindered settling.

$$w_{\text{s}} = \begin{cases} \max(w_{\text{s,min}}, 0.5w_{\text{s,max}}\ \min(2, C)), C < C_{\text{wmax}} \\ w_{\text{s,max}}\left(\max\left(0.05, \dfrac{1-\lambda_1 C^{\lambda_2}}{1-\lambda_1 C_{\text{w max}}^{\lambda_2}}\right)\right)^{4.65}, C_{\text{wmax}} < C \le C_{\text{cr}} \\ \gamma_1 C^{\delta_1}, C > C_{\text{cr}} \end{cases} \tag{8}$$

where C is the suspended sediment concentration for each class of sediment, C_{wmax} is the concentration of maximum settling velocity

Please cite this article as: Do, T.-K.-A et al., Three-dimensional numerical modeling of sediment transport in a highly turbid estuary with pronounced seasonal variations, International Journal of Sediment Research, https://doi.org/10.1016/j.ijsrc.2024.12.003

at the end of flocculation; C_{cr} is the critical concentration for the beginning of hindered settling. In the current, $C_{wmax} = 20$ g/L and $C_{cr} = 60$ g/L, $w_{s,min}$ and $w_{s,max}$ are the min and max settling velocities, respectively.

λ_1, λ_2, γ_1, and δ_1, are the constant empirical parameters, with $\lambda_1 = 0.085$ and $\lambda_2 = 0.5$. For the finer mud fraction: $w_{s,min} = 1\times 10^{-4}$ m/s; $w_{s,max} = 1 \times 10^{-3}$ m/s; $\lambda_1 = 15.74$; $\delta_1 = -3.04$. For the coarser mud fraction: $w_{s,min} = 5 \times 10^{-4}$ m/s; $w_{s,max} = 2\times 10^{-3}$ m/s; $\gamma_1 = 120.06$; $\delta_1 = -3.36$.

Recently, Defontaine et al. (2023) introduced a simple empirical formulation for the settling velocity based on field measurement data from the Garonne tidal river as described in Eq. (9):

$$w_s = 0.045C^{0.77} \tag{9}$$

The influence of salinity on flocculation also is considered when using the Le Hir et al. (2000) and Defontaine et al. (2023) formulas by modified the settling velocity according to the critical salinity as Eq. (10):

$$w_s = \begin{cases} w_s, & S \geq S_{cr} \\ \max\left(w_{s,min}, \dfrac{Sw_s}{S_{cr}}\right), & S < S_{cr} \end{cases} \tag{10}$$

where S_{cr} is the critical salinity, and S is the salinity in psu, in this study $S_{cr} = 5$ psu was chosen as a reference on the basic of previous studies (Diaz et al., 2020; Lajaunie-Salla et al., 2017).

To address the specific requirements of the current study, several key modifications are implemented in modules TELEMAC-3D and GAIA of open TELEMAC (Hervouet, 2007). These modifications included the integration of the damping function proposed by Lehfeldt and Bloss (1988), enhancements for estimating mean grain size for bedform prediction, adjustments for initializing grain size distribution and defining initial bed thickness, and custom routines for settling velocity using formulas of Le Hir et al. (2000) and Defontaine et al. (2023). Additionally, the van Rijn (2007) formula was modified to focus exclusively on the ripple and megaripple bed components. These specific adjustments were crucial for accurately representing the complex sediment dynamics and bedform characteristics of the Gironde Estuary, thereby improving the accuracy and reliability of the simulations.

3.3. Model parameterizations

A total of eight scenarios are simulated to evaluate the sensitivity of the model, as outlined in Table 1. These simulations spanned a 300-day period from January 1, 2018, to the end of October 2018, covering a wide range of river flow conditions and incorporating the two survey periods. The first scenario (RY0) simulates hydrodynamics alone (without coupling with GAIA) so that bottom friction varies spatio-temporally depending on river flow as proposed by Huybrechts et al. (2021). This scenario is used to compare the bed friction approaches and to evaluate the robustness of the bed roughness predictor proposed in the current study. The simulation RY1 for sediment transport is set up as a reference model, utilizing van Rijn (2007) bed roughness prediction and Soulsby et al. (2013) settling velocity formula, which does not require coefficients to be calibrated. In this scenario, RY1, the only parameter prescribed is the erosion coefficient (E0). The value of 0.0015 kg/m^2/s is fixed for E0 which is consistent with Diaz et al. (2020), and van Maanen and Sottolichio (2018). Subsequently, the simulation RY2 is introduced to evaluate the influence of the erosion coefficient (E0). Different scenarios are then proposed using different settling velocity formulations: van Leussen (1994) (RY3 and RY7), Le Hir et al. (2000) (RY4, RY6), and Defontaine et al. (2023) (RY5). These scenarios incorporated different numbers of sediment classes to investigate their influence on sediment transport trends.

Table 1
Model scenarios and associated parameters considered for sensitivity tests.

Run	TELEMAC-3D coupled with GAIA model	Number of cohesive class (CO)	Settling velocity formula	Erosion, E0 (kg/m^2/s^2)
RY0	No	–	–	–
RY1	Yes	1CO	Soulsby et al. (2013)	1.5E-3
RY2	Yes	1CO	Soulsby et al. (2013)	3E-3
RY3	Yes	1CO	van Leussen (1994)	1.5E-3
RY4	Yes	1CO	Le Hir et al. (2000)	1.5E-3
RY5	Yes	2CO	Defontaine et al. (2023)	1.5E-3
RY6	Yes	2CO	Le Hir et al. (2000)	1.5E-3
RY7	Yes	2CO	van Leussen (1994)	1.5E-3

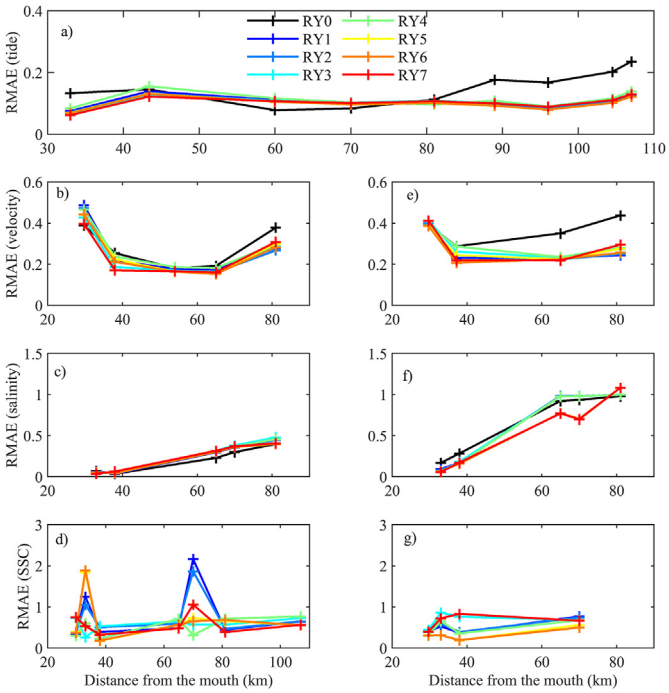

Fig. 2. RMAE estimate during low (left column) and high (right column) river flow periods for stations RY0 to RY7 along estuary.

The relative mean absolute error (RMAE) evaluates the discrepancies between the model results and the observed data. It categorizes result quality on a scale from bad to excellent: RMAE less than 0.2 is classified as excellent, RMAE between 0.2 and 0.4 is considered good, RMAE between 0.4 and 0.7 is classified as reasonable or fair, RMAE between 0.7 and 1.0 is labeled as poor, and values greater than 1.0 indicate bad performance (Sutherland et al., 2004).

$$\mathrm{RMAE} = \frac{\frac{1}{n}\sum_{i=1}^{n}|S_i - O_i|}{\frac{1}{n}\sum_{i=1}^{n}|O_i|} \tag{11}$$

where n is the total number of data; S_i and O_i are the simulated and observed values, respectively.

The calibration and sensitivity studies have been done on time series using RMAE analysis. From this RMAE analysis, a more

Please cite this article as: Do, T.-K.-A et al., Three-dimensional numerical modeling of sediment transport in a highly turbid estuary with pronounced seasonal variations, International Journal of Sediment Research, https://doi.org/10.1016/j.ijsrc.2024.12.003

limited number of runs have been selected to further investigate the ETM pattern. No additional model adjustment has been done during this analysis.

4. Results and discussions

The results of the eight scenarios are first analyzed in terms of RMAE performance. The RMAE score is estimated for the different variables: water levels, velocities, salinity, and suspended sediment concentration (SSC) to provide an overview of the model robustness. More attention is then paid on the sensitivity of the model for the SSC time variation. From RMAE and sensitivity analysis, a more restricted number of scenarios was selected. The model is further compared with SSC of *in situ* data in terms of subtidal variability. Finally, the model results are explored to determine their ability to represent the seasonal variation of the ETM location, and bottom-to-surface variations.

4.1. Model validation: sensitivity to model parameters

The results from eight sensitivity scenarios (Table 1) for water level, velocity, salinity, and SSC, are compared to observations using the RMAE index at all available stations. Fig. 2(a) shows RMAE values for nine water level stations over a 300-day period, which includes both high and low flow periods. RMAE for velocity, salinity, and SSC during low (Figs. 2(b)–2(d)) and high (Figs. 2(e)–2(g)) river flow conditions are represented separately.

The RMAE values of water levels are consistently around 0.1 (excellent) in the central part (45–80 km from the mouth, Fig. 2(a)) for the different scenarios. Some discrepancies are observed in the mouth and in the upper part of the estuary for the RY0 simulation, with RMAE greater than 0.2. Simulations RY1 to RY7 consistently have RMAE values lower than 0.15 for the 9 water level stations, highlighting the robustness of the prediction of bed roughness. Regarding current velocities, RY0 also shows less accurate velocity results in the central and upper estuary, especially for high river flow conditions, demonstrating the robustness in predicting bed roughness from the sediment transport module results in accurate reproduction of flow hydrodynamics. Otherwise, RMAE stays below 0.25 except for station P12 (Fig. 1(a)). This station is located nearshore in a cove with strong bathymetric gradients and is also exposed to wave influences.

For salinity, similar RMAE values are observed for all scenarios. During the low river flow period (Fig. 2(c)), the model features an average RMAE of 0.05 between 30 and 40 km at stations located near the river mouth. Reasonable performance (RMAE of 0.3 and 0.4) also is observed in the central and upper regions. During the high river flow period (Fig. 2(f)), all scenarios consistently reproduce salinity near the mouth and show less robust RMAE performance in the middle and upstream part of the estuary. In fact, the RMAE indicator is less accurate near the limit of saline intrusion, as salinity tends to zero and the denominator of Eq. (11) becomes small.

The comparison between modeled and measured salinity is shown in Fig. 3 for stations up to 70 km. RMAE reaches values up to 0.4–0.5 (between good and fair).

Figs. 2(d) and 2(g) show how the SSC distributions along the estuary are influenced by the model configuration. In particular, during low river flow (Fig. 2(d)), significant discrepancies between the scenarios are exhibited for both surface stations, namely at Verdon (33 km) and Pauillac (70 km, Fig. 1(a)). To highlight this discrepancy, average RMAE values of SSC during both low and high river flow periods are listed in Table 2.

Table 2 reveals that each model scenario exhibits different behavior in reproducing the SSC distribution at both the surface and the bottom. These behaviors also vary between low and high river flow periods. For all configurations, the model is more accurate for the near-bottom SSC than for the surface SSC. In particular, the RY1 and RY2 scenarios, based on the Soulsby et al. (2013) formula, as well as the two simulations involving two classes of mud (RY5 and RY6) according to the Le Hir et al. (2000) and the Defontaine et al. (2023) formulas, do not accurately reproduce the SSC pattern near the surface during low river flow (RMAE > 1). However, during high river flow, all simulations show reasonable replication of the surface SSC, with RMAE values within the range of 0.4–0.7. For the bottom SSC, all scenarios show reasonable performance during both high and low river flow periods. Interestingly, run RY1 shows the lowest RMAE value during low river flow, while RY5 and RY6 have the lowest RMAE values during high river flow.

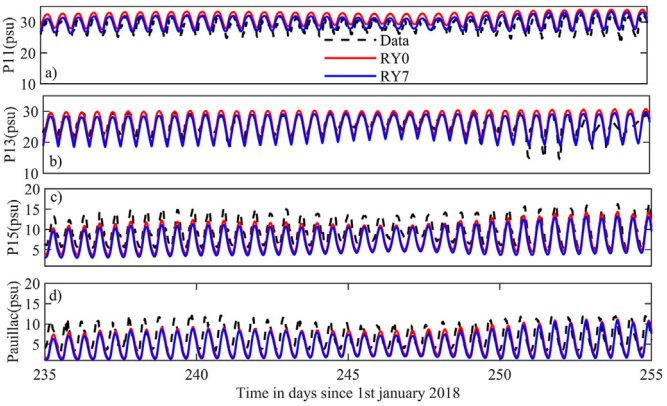

Fig. 3. Comparison between measured and modeled salinity from stations P11 to Pauillac, located respectively at 33 and 70 km from 0 km along transect A in Fig. 1(a).

When considering the averaged RMAE values for SSC along all stations, simulations based on the Le Hir et al. (2000) formulation for particle settling velocity demonstrate good performance during low and high river flow periods. In particular, the simulation RY4, which uses a single class of mud, achieves the lowest mean RMAE value of 0.52 during low river flow. During high river flow, simulations using two classes of mud (RY5 and RY6) achieve a mean RMAE of 0.33. Furthermore, the simulation that uses the van Leussen (1994) settling velocity model with two classes of mud (RY7) also performs well, although it generally has a higher mean RMAE value compared to simulations RY4 and RY6.

The relative influence of each model parameter on SSC trends is shown in (Fig. 4) for the SSC time series in the central region of the estuary, specifically at the Pauillac (surface) and P16 (bottom) stations over a cycle from winter to autumn (300 days). The sensitivity of SSC to the erosion parameter (E0) under varying river flow conditions is analyzed in scenarios RY1 and RY2 (doubled values of

Table 2
RMAE of SSC evaluated for both low and high river flow rates.

Run	Averaged RMAE for SSC at surface		Averaged RMAE for SSC at bottom		Averaged RMAE for all stations	
	Low flow	High flow	Low flow	High flow	Low flow	High flow
RY1	1.71	0.65	0.41	0.38	0.82	0.52
RY2	1.46	0.67	0.48	0.40	0.79	0.53
RY3	0.53	0.77	0.52	0.60	0.55	0.69
RY4	0.46	0.67	0.49	0.33	0.52	0.50
RY5	1.28	0.44	0.45	0.25	0.70	0.34
RY6	1.27	0.41	0.45	0.25	0.70	0.33
RY7	0.80	0.69	0.49	0.62	0.59	0.66

Please cite this article as: Do, T.-K.-A et al., Three-dimensional numerical modeling of sediment transport in a highly turbid estuary with pronounced seasonal variations, International Journal of Sediment Research, https://doi.org/10.1016/j.ijsrc.2024.12.003

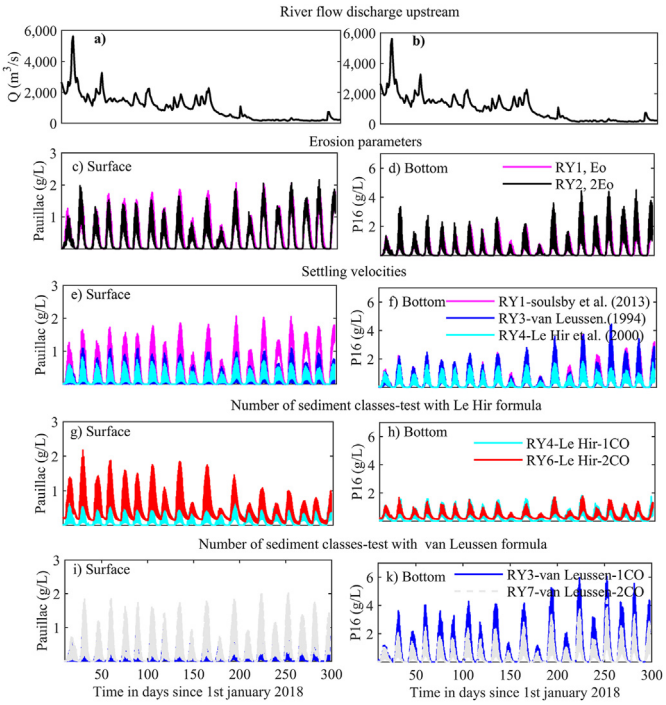

Fig. 4. Sensitivity analysis for SSC at the surface (Pauillac station) and at the bottom (P16 station).

E0), as shown in Figs. 4(c) and 4(d). The results of both simulations are quite similar. It may be expected that increasing the erosion constant tends to increase the erosion fluxes and the SSC levels. However, because deposition fluxes also are proportional to the SSC level, the combination of processes finally leads to a balance between the two fluxes, and, thus, similar levels of SSC.

The choice of settling velocities and the number of sediment classes have a more pronounced influence on the magnitude and seasonal variations of the SSC (Figs. 4(e) and 4(f)). Scenarios with the Soulsby et al. (2013) and Le Hir et al. (2000) formulations yield the highest and lowest SSC values in surface waters, respectively (Fig. 4(e)). Near the bottom, the results are relatively similar for the first 150 days. Between days of 150–300, SSC levels decrease for RY4, while the SSC levels tend to increase with RY1 and RY3. For the Le Hir et al. (2000) formulation, SSC levels during the neap tide decrease less than with only one class of mud (Figs. 4(g) and 4(h)). During spring tide, an increase in surface level is observed for RY6, whereas at the bottom, no significant differences are observed. For van Leussen (1994) formulations RY3 and RY7, the SSC levels stay low during the neap tide. The level of SSC during spring tide has increased significantly from RY3 to RY7 with depth averaged concentration values up to 5 g/L.

The RMAE analysis demonstrates the difficulty in selecting the best scenario, as the scenarios that better reproduce the observations vary according to the river flow and the water depth considered between surface and bottom. These results indicate the importance of collecting SSC data both at the surface and at the bottom to evaluate the model robustness. Surface datasets are easier to collect, but bottom datasets better represent the exchange between the bed deposit and the water column. It is, thus, chosen here to emphasize the bottom dataset rather than the surface dataset.

Sensitivity analysis indicates that the model reacts more to the settling velocity and the number of classes than the erosion constant. The model set-ups with two classes of mud have lower RMAE for SSC near the bottom than the equivalent set-ups with only one class of mud. Thus, it is proposed to further analyze three simulations with two classes of mud using the Defontaine et al. (2023) formula (RY5), the Le Hir et al. (2000) formula (RY6), and the van Leussen (1994) formula (RY7). The setup with the Soulsby et al. (2013) formulation is also kept (RY1).

4.2. Subtidal variability in the SSC pattern

Subtidal sediment dynamics play a crucial role in controlling large-scale transport patterns and budgets (Diaz et al., 2020). In this section, the subtidal variability of SSC is explored throughout the Gironde Estuary, shedding light on the influence of the settling velocity formulation. Fig. 5 shows the observed and simulated tide-averaged SSC at different stations from the mouth to the confluence, covering almost the entire period from March to October 2018, and, therefore, the varying conditions of river flow (from 150 to 2,270 m^3/s) and the tidal range (Fig. 5(a)).

The SSC measured on the surface at the Verdon and Pauillac stations tends to increase during high river flow and decrease during low river flow. A higher variation of the spring-neap is observed at Verdon during the winter compared to the summer. At the Pauillac station, the SSC measurements show fewer contrasted neap-spring fluctuations than found at the other stations. The SSC measured at the station P12 (Fig. 1(a)) does not show a clear seasonal trend, but it shows the influence of the tidal range. A larger tidal range results in a higher SSC. At the station P13, the seasonal trend in sediment dynamics also is difficult to discern and the signal also is influenced by the tidal range. The magnitude of SSC increases compared to the station P12. Data at stations P14 and P15 only are available during the low river flow period, the variation of SSC in the seasonal trend cannot be observed at these stations. However, in terms of longitudinal distribution, Fig. 5 clearly reveals the development of the higher SSC in the central part (station P16, upstream of the Pauillac station) during the low river flow period (day 254). SSC reaches 0.56 g/L at the mouth of the estuary (station P12), increases to 1 g/L at station P13, increases to 2 g/L at station P15, and reaches a maximum of 3 g/L at station P16.

Scenarios using the Defontaine et al. (2023) (RY5) and Le Hir et al. (2000) (RY6) formulas display similar results and are able to correctly reproduce SSC levels at surface stations, particularly at Verdon and also during the neap tide at Pauillac. These formulations accurately represent higher levels of SSC during periods of high river flow and a decrease in SSC during low river flow. On the contrary, the Soulsby et al. (2013) formulation (RY1) predicts stronger neap-spring variations at Pauillac, especially for the low river flow period, whereas the van Leussen (1994) scenario (RY7) produces lower levels of SSC but still features an acceptable RMAE.

All the scenarios reproduce the bottom SSC variation at stations P12 and P13, even if RY7 is less efficient for the summer at the station P12. From P13 to P16, RY1 (Soulsby et al., 2013) and RY7 (van Leussen, 1994) better reproduce the increase of the SSC level during the summer. At stations P15 and P16, simulation RY7, demonstrates better performance in reproducing bottom SSC in this region. This is indicated by the higher SSC at the station P16 compared to the station P15, similar to the observed data. On the other hand, simulation, RY5 (Defontaine et al., 2023) and RY6 (Le Hir et al., 2000) show a significant underestimation and a loss of SSC at the station P16, with lower SSC levels than at the station P15.

These results highlight the RMAE analysis providing better scores for the Le Hir et al. (2000) and Soulsby et al. (2013) formulas compared to that of van Leussen (1994). Indeed, it appears that the van Leussen (1994) formula effectively captures the seasonal dynamics of SSC and maintains SSC development during low river flow compared to simulations of using the Le Hir et al. (2000) and Soulsby et al. (2013) formulas.

Please cite this article as: Do, T.-K.-A et al., Three-dimensional numerical modeling of sediment transport in a highly turbid estuary with pronounced seasonal variations, International Journal of Sediment Research, https://doi.org/10.1016/j.ijsrc.2024.12.003

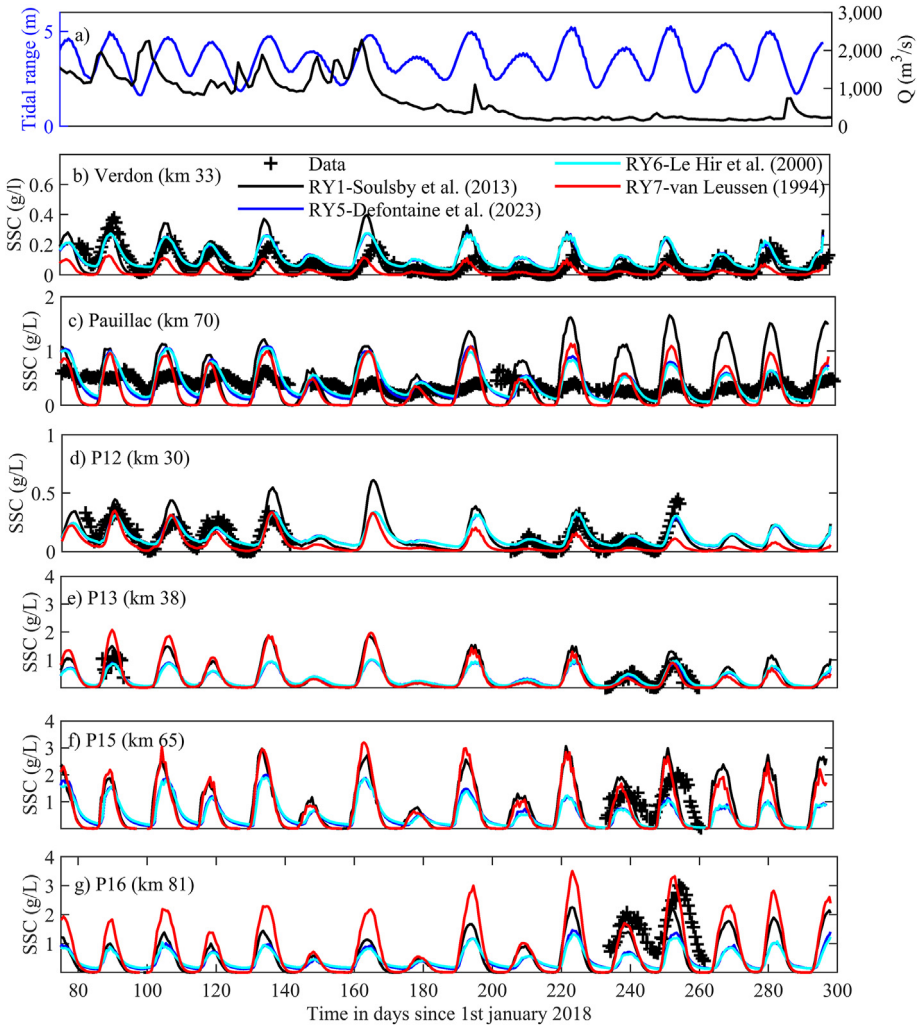

Fig. 5. (a) Time series of river flow for both Garonne and Dordogne rivers and tidal range at Verdon station; (b–g) Variation in tidal-average of SSC at different locations along the estuary (from Verdon to P16) for observations and different scenarios.

4.3. Seasonal variability in SSC pattern

During spring tides, when ETM is fully developed, seasonal variability was analyzed by examining the vertical distribution of salinity and SSC along the navigation channel (Fig. 1), as shown in Figs. 6 and 7. The variables are averaged over two spring semi-diurnal tidal cycles, during high river flow (1,700 m^3/s) and during low river flow (200 m^3/s).

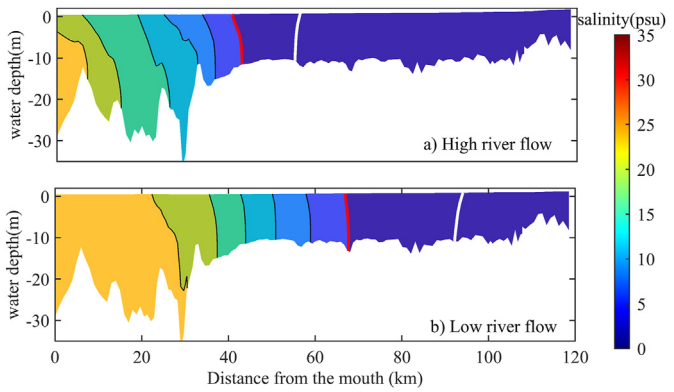

Fig. 6. Variation of salinity in the vertical along the navigation channel during (a) high and (b) low river flow for run RY7 for the spring tide condition. Iso value of 5 psu is indicated with a red line, and 0.5 psu is indicated with a white line.

The salinity distributions along the navigation channel exhibit similar patterns between scenarios with different settling velocities, so only the salinity distribution of simulation RY7 is shown in Fig. 6 for both high and low flow conditions. Salinity intrusion appears to be partially stratified, limiting intrusion near the mouth of the estuary during high river flow conditions. For example, the 5 psu isohaline propagates to a depth of 44 km at the bottom and 41 km near the surface during spring tides. During low river flow conditions, salinity enters the estuary up to the middle part of the estuary, located approximately at 70 km from 0 km according to the transect A (Fig. 1(a)), with an isohaline of 5 psu. It also penetrates part of the river, as indicated by 0.5 psu isohaline, showing a well-mixed pattern. The position of the salt front during both low and high river flow conditions aligns with the findings of van Maanen and Sottolichio (2018), who observed the salt front located in the estuary between Pauillac and Verdon during high river flow and extending into the tributaries of Garonne and Dordogne rivers during low river flow.

The influence of the settling velocity on the vertical distribution of SSC along the navigation channel is shown in Fig. 7. Simulations RY5 and RY6, using settling velocity formulae by

Please cite this article as: Do, T.-K.-A et al., Three-dimensional numerical modeling of sediment transport in a highly turbid estuary with pronounced seasonal variations, International Journal of Sediment Research, https://doi.org/10.1016/j.ijsrc.2024.12.003

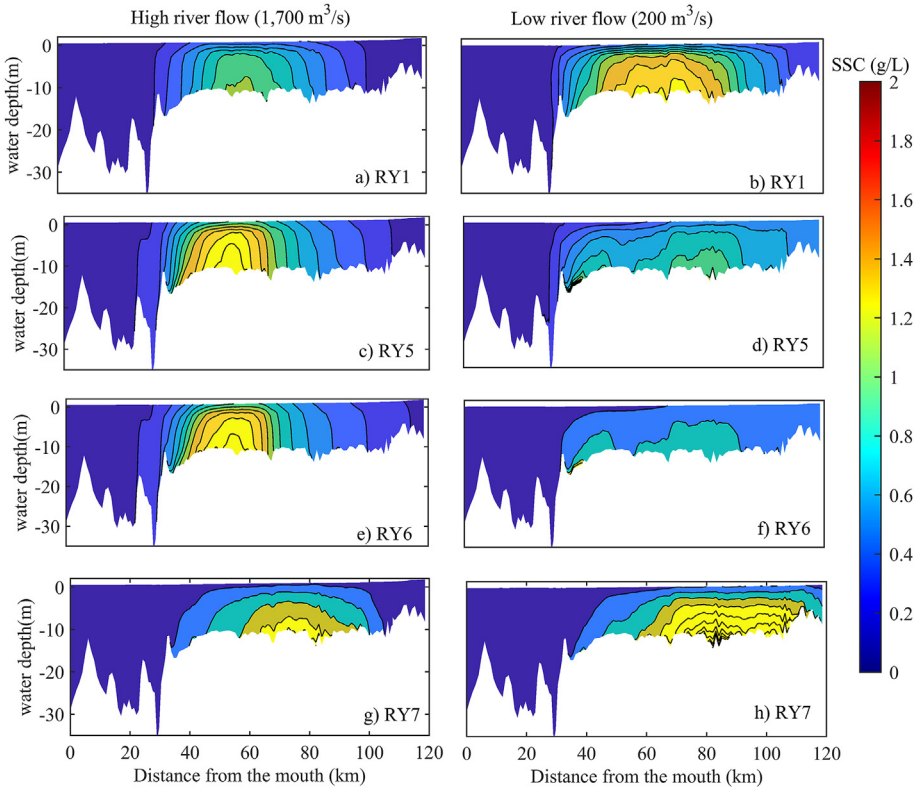

Fig. 7. Variation of SSC over water column in the vertical along the navigation channel during high and low river flow for the spring tide condition for sensitivity scenarios RY1, RY5, RY6, and RY7. A distance equal to 70 km corresponds to the location of Pauillac.

Defontaine et al. (2023) and Le Hir et al. (2000), respectively, indicate the presence of an ETM in the lower part of the estuary, located approximately at 56 km from 0 km, during periods of high river flow, with values of 2.4 and 2.3 g/L near the bottom, respectively. Furthermore, the turbidity maximum penetrates further towards the surface, with values of 1.3 and 1.2 g/L for simulations RY5 and RY6, respectively. During periods of low river flow, both simulations feature two turbidity maximum zones: one at 38 km in the lower part and another zone at around 80 km, upstream of the Pauillac station. In contrast to SSC level during high river flow conditions, there is a decrease in the magnitude of SSC. This decrease of SSC from winter to fall seasons is not consistent with *in situ* observations (Fig. 4).

In contrast, simulation RY1, using the Soulsby et al. (2013) settling velocity formula displays a higher SSC during low flow rates than during high flow rates. As indicated in Fig. 7, ETM locations stay in the central part of the estuary (40–80 km). ETM is located near the bed for the winter period, whereas much more vertical mixing is noticed for the summer with a high SSC at the surface. During high river flow, the highest maximum SSC concentration occurs near the bottom at 62 km, with a value of 1.6 g/L, while it increases to 2.2 g/L during low river flow and remains in the stretch from 62 to 73 km.

Simulation RY7, utilizing the van Leussen (1994) settling velocity formula, displays high near bed SSC levels for both seasons. Compared to the other formulations, more vertical stratification and higher near the bottom SSC are observed during the high flow rate. ETM is located from either side of 70 km Pauillac, whereas most of ETM is upstream 70 km during the low flow rate. The modeled ETM at the low flow rate is more developed up to mid depth and extends further into the upstream part of the estuary.

The location of the ETM core is estimated using the maximum value of the depth-averaged and tide-averaged SSC along the channel profile (Fig. 1(a)). Most of these maximum values are higher than 1 g/L, which is the threshold used to define ETM in the Gironde Estuary (Allen et al., 1977; Jalón-Rojas et al., 2015, 2021). Fig. 8 shows the position of the maximum SSC according to the flow rate.

Interestingly, the simulation using the Soulsby et al. (2013) formulation exhibited a relatively stable location of the ETM, approximately at 50 km during high river flow and 60 km (from 0 km according the transect A in Fig. 1(a)) during low river flow. The position of ETM using Le Hir et al. (2000) and Defontaine et al. (2023) formulas showed a similar shift, ranging from 60 km during high river flow to approximately 100 km during low river flow. The van Leussen (1994) formula indicates a shift in the maximum location further downstream during high river flow, at km 35, and moves up to 80 and 100 km under low river flow. As already pointed out, the magnitude of the SSC remains high during low and high river flow for scenario RY7 whereas the SSC levels decrease significantly for scenario RY5 and RY6.

4.4. Surface–bottom variation

The spatial distributions of SSC under seasonal variation within the Gironde Estuary have been investigated using either a numerical model (van Maanen & Sottolichio, 2018) or satellite image data (Doxaran et al., 2009; Normandin et al., 2019). However, these studies only highlighted the surface SSC distribution and the variation between surface and bottom patterns were less described. Here this variation is investigated for scenarios RY6 (Le Hir et al. (2000)) and RY7 (van Leussen (1994)) featuring contrasting vertical patterns (Fig. 7).

Please cite this article as: Do, T.-K.-A et al., Three-dimensional numerical modeling of sediment transport in a highly turbid estuary with pronounced seasonal variations, International Journal of Sediment Research, https://doi.org/10.1016/j.ijsrc.2024.12.003

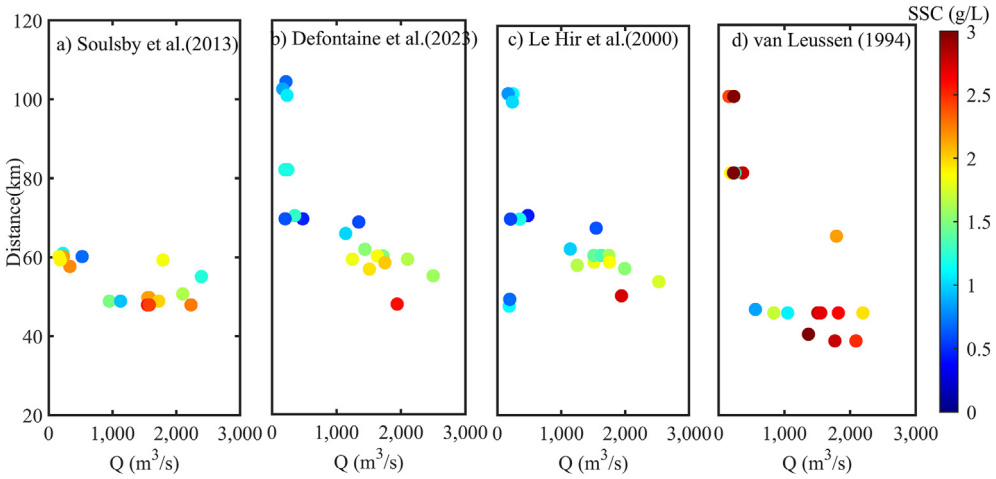

Fig. 8. ETM locations as a function of different river flow rates for scenarios RY1 (Soulsby et al. (2013)), RY5 (Defontaine et al. (2023)), RY6 (Le Hir et al. (2000)), and RY7 (van Leussen (1994)). Colored points correspond to SSC magnitude indicated in the colorbar at left.

The seasonal variations of fluid mud deposits (the cumulative thickness comprises the five first bed layers, with concentration values ranging from 66 to 330 g/L) are plotted in Fig. 9 to analyze the influence of the settling velocity on the exchange between the water column and the bed deposit. To represent the low river flow period, an average of 33 simulated frames was selected, with daily flow ranging from 98 to 252 m^3/s, corresponding to an average of 149 m^3/s, during five spring periods at low tide. Similarly, an average of 24 simulated frames, with daily flow ranging from 850 to 1,700 m^3/s, corresponding to an average of 1,143 m^3/s, during spring periods at low tide, were selected to represent the high river flow period.

The pattern of seasonal variation of the fluid mud thickness is consistent between the two scenarios (RY6 and RY7), but shows discrepancy in terms of magnitude. For scenario RY6, the tidal averaged thicknesses of fluid mud are less than 0.2 m for both hydrological regimes. Magnitudes are higher for scenario RY7, as tidal averaged fluid mud thicknesses reached 0.4 m.

During high river flow, the fluid mud is located mainly within 40–100 km with the highest level between 65 and 90 km, as shown in Fig. 9(b) (the continuous line indicates the average thickness of mud during high river flow). However, during low river flow, the mud deposit downstream of 80 km is eroded and a higher mud thickness is observed upstream (110 km), corresponding to a higher concentration ETM in this zone.

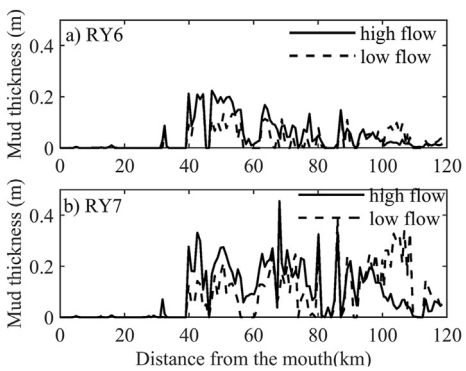

Fig. 9. Variation of tidal averaged fluid mud thickness along navigation channel during high and low river flow (a) scenario RY6 and (b) scenario RY7.

Figs. 10 and 11 show the averaged distribution of the surface and the bottom SSC during high and low river flow periods at low tide and during spring conditions. During periods of low river flow, both simulations indicate highest SSC values at the surface in the tributaries, as shown in Figs. 10(a) and 11(a). The near-bottom SSC pattern in the scenario RY6 (Fig. 10(c)) appears to be distributed along the entire estuary with slightly higher values on both sides of Pauillac with a second plume in the tributaries. Higher levels of bottom SSC in scenario RY7 (Fig. 11(c)) are continuously observed from the central part around Pauillac to upstream of the Bordeaux station.

For scenario RY6, a sole turbid plume is observed with a core having shifted downstream of Pauillac and high SSC both at the bottom or water surface during high river flow. In contrast, the scenario RY7 predicts near the bottom two turbid plumes either at

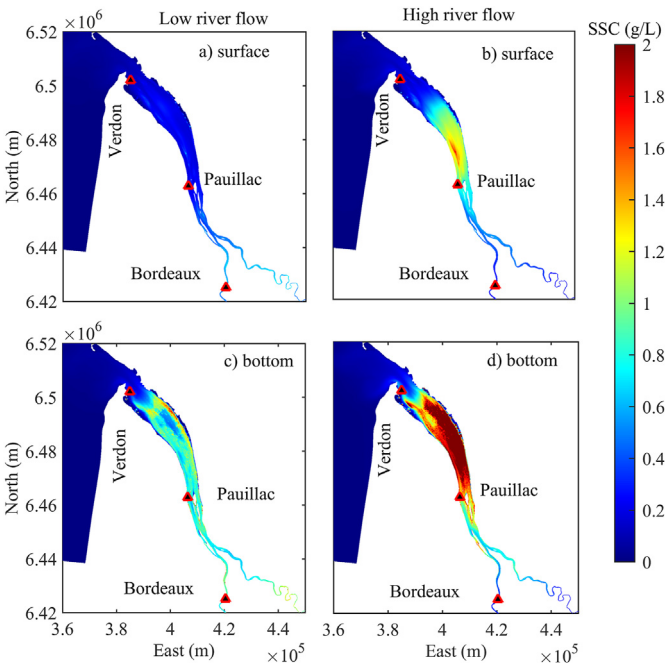

Fig. 10. Surface and bottom SSC distribution during low and high river flow of simulation RY6 (Le Hir et al. (2000) formula).

Please cite this article as: Do, T.-K.-A et al., Three-dimensional numerical modeling of sediment transport in a highly turbid estuary with pronounced seasonal variations, International Journal of Sediment Research, https://doi.org/10.1016/j.ijsrc.2024.12.003

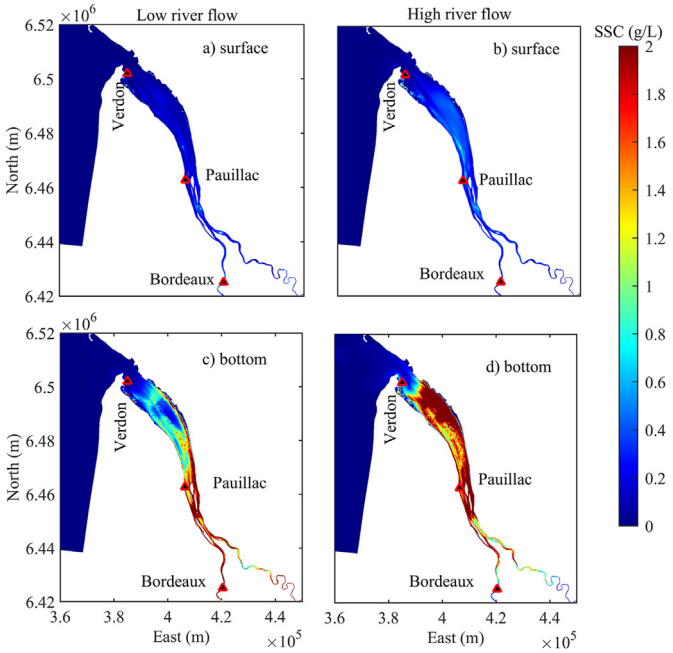

Fig. 11. Surface and bottom SSC distribution during low and high river flow of simulation RY7 (van Leussen (1994) formula).

the mouth and around Pauillac. On the surface the highest values are noticed downstream of the Pauillac station near the navigation channel.

For river discharges ranging from 154 to 270 m^3/s during low flow rate periods, the turbidity maximum zone clearly extends further upstream and extends across the central part of the area, spanning from 60 to 120 km, with a maximum concentration of the ETM exceeding 1 g/L (Fig. 10(d)). The location of the turbidity maximum remains relatively stable during this period, with its magnitude being influenced by the tidal range rather than the river discharge. Larger tidal ranges induce higher ETM concentrations, underscoring the stronger role of tides in ETM development and upstream movement under conditions of low river flow.

In comparison, van Maanen and Sottolichio (2018) observed the stable turbidity maximum zone near the surface that occurs near the Pauillac station and other locations in riverine areas based on simulations in 2015 with an average monthly discharge of approximately 400 m^3/s. Meanwhile, Normandin et al. (2019) observed the turbidity maximum in the riverine area during low tidal ranges and upstream of Pauillac during high tidal ranges (Figs. 6(e) and 6(f), Normandin et al., 2019) under conditions of low river discharge. Normandin et al. (2019) pointed out that the maximum turbidity develops along the navigation channel further in the tributaries (near Bordeaux station) during the summer (average discharge of 267 m^3/s) and autumn seasons (average discharge of 399 m^3/s). The surface development of the simulated turbidity maximum in the tributaries found in the current study is consistent with previous studies.

For the distribution of SSC near the bottom during this low flow period, simulation RY7 using the van Leussen (1994) settling velocity formula, exhibits a high degree of consistency with the observations of Diaz et al. (2020). The authors applied a three-day numerical filter during neap tide conditions in both April 2015 (for high river discharge) and late August 2015 (for low river discharge). This alignment is particularly notable because it indicates that the location of the maximum turbidity is consistently observed near the Pauillac station. Furthermore, the simulation RY7 outperforms other simulations in reproducing SSC levels at the station P16. This can be observed in Fig. 5(g), which shows a comparison of the tidal averages of SSC between the simulation and the observations.

During high river discharge conditions, ETM shifts toward the lower part of the estuary downstream of the Pauillac station, both near the surface and near the bottom in simulation RY6. In contrast, the simulation RY7 reveals the presence of two ETM. One remains near the Pauillac station, similar to its occurrence during low river flow, forming a stable zone. The other, a dynamic zone, is observed to change downstream near the riverbank. The distribution observed in simulation RY7 is consistent with the findings of previous studies (Diaz et al., 2020; Lajaunie-Salla et al., 2017; Normandin et al., 2019; van Maanen & Sottolichio, 2018). Even if RY7 has a slightly higher RMAE than the other scenarios, it features higher bed deposition which seems more consistent with the dredging activities, and this scenario appears the most robust to reproduce the seasonal variation and the migration of the turbidity maximum from downstream to upstream.

4.5. Implications for other estuaries, limitations, and perspectives

The findings of the current study have wide-reaching implications for estuarine research and management. First, the enhanced model validation achieved by coupling hydrodynamics with sediment transport, incorporating feedback on bed friction and bottom depth changes, underscores the relevance of this approach in highly turbid systems undergoing rapid shifts in sediment patterns and morphology. This advancement represents a critical step forward in modeling hydro-sedimentary processes, particularly in the context of climate change, where estuarine processes evolve over time (Grasso & Caillaud, 2023; Jalón-Rojas et al., 2021) and the calibration of hydrodynamics at a given period may prove insufficient for predicting environmental conditions under different scenarios. In this sense, future studies may also include the effect of sediment-induced density effects on hydrodynamics as these can impact tidal asymmetry and consequently tidal pumping and ETM dynamics, as proposed by Zhu et al. (2022).

Second, the reduction of calibration parameters proposed in the current study has mitigated the equifinality problem that typically affects this type of study, wherein multiple parameter sets can produce similar model outputs (Diaz et al., 2020; van Maren & Cronin., 2016). Compared to previous studies, e.g., Diaz et al. (2020), the proposed approach requires fewer calibrated parameters, which enhances model robustness and reduces the risk of equifinality. The parameters that did not require calibration include bed roughness, critical shear stresses for erosion, and transfer coefficients for consolidation. The only two tuned parameters are the erosion parameter, E0, and the settling velocity, w_s, when the van Leussen (1994) formula is used. Despite this reduction that improves the robustness of the model and increases confidence in the selected parameterization, the sensitivity test utilizing different settling velocity approaches and sediment classes highlights the persistence of some uncertainty and the need for careful consideration of model configurations. For example, the observed influence of some approaches on the location and magnitude of the ETM emphasizes the importance of selecting an appropriate settling velocity formulation. This decision may not be straightforward, and comparisons of observations and simulations should be made at different temporal and spatial scales using long-term time series. The relevance of using such a long-term dataset has also been highlighted in recent studies, e.g., Winterwerp et al. (2021).

Future research will focus on modeling hydro-sedimentary dynamics in the Gironde's tidal rivers and outer plume, aiming to encompass the full continuum from land to sea. This expansion will

Please cite this article as: Do, T.-K.-A et al., Three-dimensional numerical modeling of sediment transport in a highly turbid estuary with pronounced seasonal variations, International Journal of Sediment Research, https://doi.org/10.1016/j.ijsrc.2024.12.003

specifically address the challenges and complexities associated with narrower tidal river systems, considering factors such as channel geometry, bathymetry, tidal-river dynamics, and hydro-morphosedimentary feedbacks. The insights gained from this extended modeling effort will contribute to a more comprehensive framework applicable not only to the Gironde Estuary but also to other turbid systems worldwide, enhancing the understanding of estuarine and coastal sediment transport processes.

5. Conclusions

In the current study, a realistic 3D numerical model was developed to examine the dynamics of SSC in the Gironde Estuary, a complex estuarine environment characterized by a strong tidal range and significant variations in river discharge. The numerical model uses the open TELEMAC system to simulate the hydrodynamics and sediment transport, taking into account the movement of the sand-mud mixtures. The proposed methodology features three main original concepts: 1) it has coupled bed friction in the hydrodynamic model with mixed sediment transport, enabling feedback on bed roughness and changes in bottom depth; 2) it has applied a calibration strategy that reduces the calibrated parameters as much as possible, relies on *in situ* input data, and encompasses hydro−morpho-sedimentary interactions; 3) it has analyzed the ability of the model to represent upstream migration of ETM.

The hydrodynamic results were compared with field surveys of water level, velocity, and salinity during low and high river flow periods. The bed roughness evolves in space and time according to the sediment transport and the associated evolutions of the grain distribution. This approach based on the bed roughness prediction appears to be efficient to maintain an accurate prediction of the water levels and velocities during the high and low flow periods.

The proposed methodology relies as much as possible on measured data to avoid the issue of equifinality. The non-calibrated parameters are the bed friction, the critical shear stress for erosion, transfer coefficient for consolidation. The two required parameters are the erosion constant, E0, and the settling velocity.

Comparing the model results with observations reveals that the model accurately reproduces the seasonal trend of SSC and the formation of a well-defined turbidity maximum. An evident high turbidity zone is formed and moves downstream during high river flow, while moving upstream under low river flow conditions, which is consistent with previous studies. Furthermore, the model also effectively reproduces the observed variations in SSC during the spring-neap tidal cycle, particularly at the river mouth and in the central part of the estuary (locations P12, P13, P15, and P16). During spring tides, the higher concentration of SSC and the formation of the turbidity maximum zone are attributed to more intense turbulent conditions. In contrast, SSC concentrations are significantly lower during neap tides compared to spring tides, regardless of high or low river flow conditions due to lower velocity and lower resuspension.

A sensitivity study reveals that the settling velocity plays a crucial role in determining the magnitude, location, and formation of the turbidity maximum zone. With the settling velocity formulation of Soulsby et al. (2013) only the erosion coefficient needs to be specified. However, it appears that this approach predicts an ETM staying within 50−60 km for high and low flow rates which is not consistent with previous observations. The two empirical formulas proposed by Le Hir et al. (2000) and Defontaine et al. (2023) indicate a loss in SSC concentration when long-time simulations are done, thereby underestimating SSC levels during low river flow. This discrepancy can be attributed to the difficulty in maintaining the equilibrium turbidity maximum, as previously observed by Diaz et al. (2020) and Orseau et al. (2021). However, the two classes of mud simulations presented by Le Hir et al. (2000) and Defontaine et al. (2023) improve the turbidity levels during neap tides, although they still underestimate the observed values. The van Leussen (1994) formula appears as the most efficient as it has well-reproduced the seasonal dynamics of the turbidity maximum's development and exhibits the ability to sustain a high turbidity maximum while the maximum migrates further upstream during low river flow.

Declaration of competing interest

The authors declare that they have no known competing financial interests or personal relationships that could have appeared to influence the work reported in this paper.

CRediT authorship contribution statement

Thi-Kim-Anh Do: Writing − review & editing, Writing − original draft, Visualization, Validation, Methodology, Formal analysis, Conceptualization. **Nicolas Huybrechts:** Writing − review & editing, Writing − original draft, Validation, Supervision, Software, Project administration, Methodology, Investigation, Funding acquisition, Formal analysis. **Isabel Jálon-Rojas:** Writing − review & editing, Writing − original draft, Investigation, Conceptualization. **Pablo Tassi:** Writing − review & editing, Software, Conceptualization. **Aldo Sottolichio:** Writing − review & editing, Funding acquisition, Conceptualization.

Acknowledgements

The authors would like to thank Service Hydrographique Marine (SHOM) for the digital elevation model (DEM) of the Gironde Estuary, Agence de l'eau for the suspended sediment concentration (SSC) data (Naiades), Direction Régionale de l'Environnement, de l'Aménagement et du Logement (DREAL) for the flow rate data. This research has been done during the EMPHASE project funded by l'Agence Nationale de la Recherche and Les Fonds de Recherche du Québec (ANR-FRQ) program under grant ARN-19-FQSM-0003-01. Mooring at stations P11 to P16 have been done with funding from the Connecting Europe Facility (CEF)—Transport Sector under agreement (Innovation and Networks Executive Agency) Grant No. INEA/CEF/TRAN/M2014/1049680 through the project Gironde XL. The authors also would like to thank the Grand Port Maritime of Bordeaux (GPMB) for providing the bathymetry data along the navigation channel.

References

Abascal-Zorrilla, N., Vantrepotte, V., Huybrechts, N., Ngoc, D. D., Anthony, E. J., & Gardel, A. (2020). Dynamics of the estuarine turbidity maximum zone from Landsat-8 data: The case of the Maroni River estuary, French Guiana. *Remote Sensing, 12*(13), 2173.

Allen, G. P., Salomon, J. C., Bassoullet, P., Du Penhoat, Y., & De Grandpre, C. (1980). Effects of tides on mixing and suspended sediment transport in macrotidal estuaries. *Sedimentary Geology, 26*(1−3), 69−90.

Allen, G. P., Sauzay, G., & Castaing, P. (1977). Transport and deposition of suspended sediment in the Gironde Estuary, France. In M. Wiley (Ed.), *Estuarine processes* (pp. 63−81). New York: Academic Press.

Beven, K., & Freer, J. (2001). A dynamic topmodel. *Hydrological Processes, 15*(10), 1993−2011.

Bonnefille, R. (1971). Remarques sur les écoulements moyens à l'aval de la Gironde. *Bulletin de l'Institut de Geologie du Bassin d'Aquitaine, 11*, 361−364. *(in French)*

Brenon, I., & Le Hir, P. (1999). Modelling the turbidity maximum in the Seine Estuary (France): Identification of formation processes. *Estuarine, Coastal and Shelf Science, 49*(4), 525−544.

Burchard, H., & Baumert, H. (1998). The formation of estuarine turbidity maxima due to density effects in the salt wedge: A hydrodynamic process study. *Journal of Physical Oceanography, 28*(2), 309−321.

Please cite this article as: Do, T.-K.-A et al., Three-dimensional numerical modeling of sediment transport in a highly turbid estuary with pronounced seasonal variations, International Journal of Sediment Research, https://doi.org/10.1016/j.ijsrc.2024.12.003

Castaing, P., & Allen, G. P. (1981). Mechanisms controlling seaward escape of suspended sediment from the Gironde: A macrotidal estuary in France. *Marine Geology, 40*(1–2), 101–118.

Chen, D., Zheng, J., Zhang, C., Guan, D., Li, Y., & Wang, Y. (2021). Critical shear stress for erosion of sand-mud mixtures and pure mud. *Frontiers in Marine Science, 8*, 713039.

Chini, N., & Villaret, C. (2007). Numerical modelling of the bed evolution downstream of a dike in the Gironde estuary. In *Proceedings of the river, coastal and estuarine morphodynamics conference*. Didcot, UK: Taylor & Francis.

Chou, Y. J., Nelson, K. S., Holleman, R. C., Fringer, O. B., Stacey, M. T., Lacy, J. R., & Koseff, J. R. (2018). Three-dimensional modeling of fine sediment transport by waves and currents in a shallow estuary. *Journal of Geophysical Research: Oceans, 123*(6), 4177–4199.

Coynel, A. (2005). *Erosion mécanique des sols et transferts géochimiques dans le bassin Adour-Garonne*. University of Bordeaux I.. Doctoral dissertation. (in French).

Coynel, A., Blanc, G., Dutruch, L., Bossy, C., Lerat, A., Gil-Diaz, T., Pereto, C., Amorich, L., & Schäfer, J. (2018). Évolution des flux de MES (1994–2016) et de cadmium (1999–2016) dans le système Riou-Mort-Lot-Garonne. *Rapport contrat AEAG*, 24p. *(in French)*

Coynel, A., Schäfer, J., Hurtrez, J. E., Dumas, J., Etcheber, H., & Blanc, G. (2004). Sampling frequency and accuracy of SPM flux estimates in two contrasted drainage basins. *Science of the Total Environment, 330*(1–3), 233–247.

Defontaine, S., Jalon-Rojas, I., Sottolichio, A., Gratiot, N., & Legout, C. (2023). Settling dynamics of cohesive sediments in a highly turbid tidal river. *Marine Geology, 457*, 106995.

Diaz, M., Grasso, F., Le Hir, P., Sottolichio, A., Caillaud, M., & Thouvenin, B. (2020). Modeling mud and sand transfers between a macrotidal estuary and the continental shelf: Influence of the sediment transport parameterization. *Journal of Geophysical Research: Oceans, 125*(4), e2019JC015643.

Doxaran, D., Froidefond, J. M., Castaing, P., & Babin, M. (2009). Dynamics of the turbidity maximum zone in a macrotidal estuary (the Gironde, France): Observations from field and MODIS satellite data. *Estuarine, Coastal and Shelf Science, 81*(3), 321–332.

Druine, F., Verney, R., Deloffre, J., Lemoine, J. P., Chapalain, M., Landemaine, V., & Lafite, R. (2018). *In situ* high frequency long term measurements of suspended sediment concentration in turbid estuarine system (Seine Estuary, France): Optical turbidity sensors response to suspended sediment characteristics. *Marine Geology, 400*, 24–37.

Dyer, K. R. (1988). Fine sediment particle transport in estuaries. In *Physical processes in estuaries* (pp. 295–310). Berlin, Heidelberg: Springer Berlin Heidelberg.

Etcheber, H., Schmidt, S., Sottolichio, A., Maneux, E., Chabaux, G., Escalier, J. M., … Castaing, P. (2011). Monitoring water quality in estuarine environments: Lessons from the MAGEST monitoring program in the Gironde fluvial-estuarine system. *Hydrology and Earth System Sciences, 15*(3), 831–840.

Fettweis, M., Riethmüller, R., Verney, R., Becker, M., Backers, J., Baeye, M., … Vereecken, H. (2019). Uncertainties associated with *in situ* high-frequency long-term observations of suspended particulate matter concentration using optical and acoustic sensors. *Progress in Oceanography, 178*, 102162.

Flores, R. P., Rijnsburger, S., Horner-Devine, A. R., Kumar, N., Souza, A. J., & Pietrzak, J. D. (2020). The formation of turbidity maximum zones by minor axis tidal straining in regions of freshwater influence. *Journal of Physical Oceanography, 50*(5), 1265–1287.

Fuentes-Cid, A., Etcheber, H., Schmidt, S., Abril, G., De-Oliveira, E., Lepage, M., & Sottolichio, A. (2014). Dynamics of coarse particulate matter in the turbidity maximum zone of the Gironde Estuary. *Comptes Rendus Geoscience, 346*(1–2), 28–36.

Geyer, W. R. (1993). The importance of suppression of turbulence by stratification on the estuarine turbidity maximum. *Estuaries, 16*, 113–125.

G.P.M.B. (2002). *Demande d'autorisation pour l'entretien du chenal et des ouvrages portuaires et pour l'amélioration du chenal*. Octobre: Chenal de Navigation et Ouvrages Portuaires. *(In French)*

Grasso, F., & Caillaud, M. (2023). A ten-year numerical hindcast of hydrodynamics and sediment dynamics in the Loire Estuary. *Scientific Data, 10*(1), 394.

Hervouet, J. M. (2007). *Hydrodynamics of free surface flows: Modelling with the finite element method*. John Wiley & Sons, Ltd.

Hesse, R. F., Zorndt, A., & Fröhle, P. (2019). Modelling dynamics of the estuarine turbidity maximum and local net deposition. *Ocean Dynamics, 69*, 489–507.

Huybrechts, N., Smaoui, H., Orseau, S., Tassi, P., & Klein, F. (2021). Automatic calibration of bed friction coefficients to reduce the influence of seasonal variation: Case of the Gironde estuary. *Journal of Waterway, Port, Coastal, and Ocean Engineering, 147*(3), 05021004.

Huybrechts, N., Villaret, C., & Lyard, F. (2012). Optimized predictive two-dimensional hydrodynamic model of the Gironde Estuary in France. *Journal of Waterway, Port, Coastal, and Ocean Engineering, 138*(4), 312–322.

Jalón-Rojas, I., Dijkstra, Y. M., Schuttelaars, H. M., Brouwer, R. L., Schmidt, S., & Sottolichio, A. (2021). Multidecadal evolution of the turbidity maximum zone in a macrotidal river under climate and anthropogenic pressures. *Journal of Geophysical Research: Oceans, 126*(5), e2020JC016273.

Jalón-Rojas, I., Sottolichio, A., Hanquiez, V., Fort, A., & Schmidt, S. (2018). To what extent multidecadal changes in morphology and fluvial discharge impact tide in a convergent (turbid) tidal river. *Journal of Geophysical Research: Oceans, 123*(5), 3241–3258.

Jalón-Rojas, I., Schmidt, S., & Sottolichio, A. (2015). Turbidity in the fluvial Gironde estuary (southwest France) based on 10-year continuous monitoring: Sensitivity to hydrological conditions. *Hydrology and Earth System Sciences, 19*(6), 2805–2819.

Jalón-Rojas, I., Schmidt, S., Sottolichio, A., & Bertier, C. (2016). Tracking the turbidity maximum zone in the Loire estuary (France) based on a long-term, high-resolution and high-frequency monitoring network. *Continental Shelf Research, 117*, 1–11.

Jouanneau, J. M., & Latouche, C. (1981). The Gironde estuary. *Contributions to Sedimentology, 10* (Stuttgart, Schweizerbart)

Krone, R. B. (1962). Flume studies of transport of sediment in estuarial shoaling processes. In *Final report, hydraulics engineering and sanitary engineering, research laboratory*. University of California.

Lajaunie-Salla, K., Wild-Allen, K., Sottolichio, A., Thouvenin, B., Litrico, X., & Abril, G. (2017). Impact of urban effluents on summer hypoxia in the highly turbid Gironde Estuary, applying a 3D model coupling hydrodynamics, sediment transport, and biogeochemical processes. *Journal of Marine Systems, 174*, 89–105.

Le Hir, P., Bassoullet, P., & Jestin, H. (2000). Application of the continuous modeling concept to simulate high-concentration suspended sediment in a macrotidal estuary. *Proceedings in Marine Science, 3*, 229–247.

Lehfeldt, R., & Bloss, S. (1988). Algebraic turbulence model for stratified tidal flows. In *Physical processes in estuaries* (pp. 278–291). Berlin, Heidelberg: Springer Berlin Heidelberg.

Matos, T., Faria, C. L., Martins, M. S., Henriques, R., Gomes, P. A., & Goncalves, L. M. (2020). Design of a multipoint cost-effective optical instrument for continuous in-situ monitoring of turbidity and sediment. *Sensors, 20*(11), 3194.

McSweeney, J. M., Chant, R. J., Wilkin, J. L., & Sommerfield, C. K. (2017). Suspended-sediment impacts on light-limited productivity in the Delaware Estuary. *Estuaries and Coasts, 40*, 977–993.

Meyer-Peter, E., & Müller, R. (1948). Formulas for bedload transport. In *Proceedings of the 2nd meeting of the international association for hydraulic structures research* (pp. 39–64). Stockholm: IAHR.

Nikuradse, J. (1933). Stromungsgesetze in Rauhem Rohren. *Laws of Turbulent Pipe Flow in Smooth Pipes.) VDI-Forschungsheft: Germany, 361. (in German) (Translated in NACA Tech. Memo. No. 1292, 1050*

Normandin, C., Lubac, B., Sottolichio, A., Frappart, F., Ygorra, B., & Marieu, V. (2019). Analysis of suspended sediment variability in a large highly turbid estuary using a 5-year-long remotely sensed data archive at high resolution. *Journal of Geophysical Research: Oceans, 124*(11), 7661–7682.

Orseau, S., Huybrechts, N., Tassi, P., Van Bang, D. P., & Klein, F. (2021). Two-dimensional modeling of fine sediment transport with mixed sediment and consolidation: Application to the Gironde Estuary, France. *International Journal of Sediment Research, 36*(6), 736–746.

Pairaud, I. L., Lyard, F., Auclair, F., Letellier, T., & Marsaleix, P. (2008). Dynamics of the semi-diurnal and quarter-diurnal internal tides in the Bay of Biscay. Part 1: Barotropic tides. *Continental Shelf Research, 28*(10–11), 1294–1315.

Partheniades, E. (1965). Erosion and deposition of cohesive soils. *Journal of the Hydraulics Division, 91*(1), 105–139. ASCE.

Ross, L., Huguenard, K., & Sottolichio, A. (2019). Intratidal and fortnightly variability of vertical mixing in a macrotidal estuary: The Gironde. *Journal of Geophysical Research: Oceans, 124*(4), 2641–2659.

Roy, C. J., & Oberkampf, W. L. (2011). A comprehensive framework for verification, validation, and uncertainty quantification in scientific computing. *Computer Methods in Applied Mechanics and Engineering, 200*(25–28), 2131–2144.

Saari, H. K., Schmidt, S., Castaing, P., Blanc, G., Sautour, B., Masson, O., & Cochran, J. K. (2010). The particulate 7Be/210Pbxs and 234Th/210Pbxs activity ratios as tracers for tidal-to-seasonal particle dynamics in the Gironde Estuary (France): Implications for the budget of particle-associated contaminants. *Science of the Total Environment, 408*(20), 4784–4794.

Santoro, P., Fossati, M., Tassi, P., Huybrechts, N., Van Bang, D. P., & Piedra-Cueva, I. (2019). Effect of self-weight consolidation on a hydro-sedimentological model for the Río de la Plata Estuary. *International Journal of Sediment Research, 34*(5), 444–454.

Savoye, N., David, V., Morisseau, F., Etcheber, H., Abril, G., Billy, I., … Sautour, B. (2012). Origin and composition of particulate organic matter in a macrotidal turbid estuary: The Gironde Estuary, France. *Estuarine, Coastal and Shelf Science, 108*, 16–28.

Schmidt, S. (2020). A 14-year multi-sites and high-frequency monitoring of salinity in the tidal Garonne River (SW France) reveals marked inter-annual variability in marine intrusion. In *Estuaries and coastal zones in times of global change: Proceedings of ICEC-2018* (pp. 3–11). Singapore Springer.

Schubel, J. R. (1968). Turbidity maximum of the northern Chesapeake Bay. *Science, 161*(3845), 1013–1015.

Sottolichio, A. (1999). *Modélisation de la dynamique des structures turbides (bouchon vaseux et crème de vase) dans l'estuaire de la Gironde*. University of Bordeaux I.. Doctoral dissertation. (in French).

Sottolichio, A., & Castaing, P. (1999). A synthesis on seasonal dynamics of highly-concentrated structures in the Gironde Estuary. *Comptes Rendus de l'Academie des Sciences - Series IIA: Earth and Planetary Science, 329*(11), 795–800.

Sottolichio, A., Le Hir, P., & Castaing, P. (2000). Modeling mechanisms for the stability of the turbidity maximum in the Gironde estuary, France. In *Proceedings in marine science* (Vol. 3, pp. 373–386). Amsterdam: Elsevier.

Soulsby, R. L., Manning, A. J., Spearman, J., & Whitehouse, R. J. S. (2013). Settling velocity and mass settling flux of flocculated estuarine sediments. *Marine Geology, 339*, 1–12.

Sutherland, J., Peet, A. H., & Soulsby, R. (2004). Evaluating the performance of morphological models. *Coastal Engineering, 51*(8–9), 917–939.

Please cite this article as: Do, T.-K.-A et al., Three-dimensional numerical modeling of sediment transport in a highly turbid estuary with pronounced seasonal variations, International Journal of Sediment Research, https://doi.org/10.1016/j.ijsrc.2024.12.003

Talke, S. A., & Jay, D. A. (2020). Changing tides: The role of natural and anthropogenic factors. *Annual Review of Marine Science, 12*, 121–151.

Tassi, P., Benson, T., Delinares, M., Fontaine, J., Huybrechts, N., Kopmann, R., … Walther, R. (2023). Gaia - a unified framework for sediment transport and bed evolution in rivers, coastal seas, and transitional waters in the TELEMAC-MASCARET modelling system. *Environmental Modelling & Software, 159*, 105544.

Van, L. A. (2012). *Numerical modelling of sand-mud mixtures settling and transport processes: Application to morphodynamics of the Gironde estuary (France)*. Université Paris-Est.. Doctoral dissertation.

van Leussen, W. (1994). *Estuarine macroflocs and their role in fine-grained sediment transport*. University of Utrecht.. Doctoral dissertation.

van Maanen, B., & Sottolichio, A. (2018). Hydro- and sediment dynamics in the Gironde Estuary (France): Sensitivity to seasonal variations in river inflow and sea level rise. *Continental Shelf Research, 165*, 37–50.

van Maren, D. S., & Cronin, K. (2016). Uncertainty in complex three-dimensional sediment transport models: Equifinality in a model application of the Ems Estuary, The Netherlands. *Ocean Dynamics, 66*, 1665–1679.

van Rijn, L. C. (2007). Unified view of sediment transport by currents and waves. I: Initiation of motion, bed roughness, and bed-load transport. *Journal of Hydraulic Engineering, 133*(6), 649–667.

Villaret, C., Huybrechts, N., Davies, A. G., & Way, O. (2011). Effect of bed roughness prediction on morphodynamic modelling: Application to the dee estuary (UK) and to the Gironde estuary (France). In *Proceedings of the 34th world congress of the international association for hydro-environment research and engineering: 33rd hydrology and water resources symposium and 10th conference on hydraulics in water engineering* (pp. 1149–1156). Engineers Australia: Barton, ACT.

Waeles, B. (2005). *Modélisation morphodynamique de l'embouchure de la Seine*. Université de Caen Basse-Normandie.. Doctoral dissertation. (in French).

Winterwerp, J. C., van Kessel, T., van Maren, D. S., & van Prooijen, B. C. (2021). Fine sediment in open water: From fundamentals to modeling. *Advance Series in Ocean Engineering, 55* (World Scientific)

Winterwerp, J. C., & van Kesteren, W. G. (2004). *Introduction to the physics of cohesive sediment dynamics in the marine environment*. Amsterdam: Elsevier.

Zhang, S., Nielsen, P., Perrochet, P., Xu, B., Jia, Y., & Wen, M. (2021). Derivation of settling velocity, eddy diffusivity and pick-up rate from field-measured suspended sediment concentration profiles in the horizontally uniform but vertically unsteady scenario. *Applied Ocean Research, 107*, 102485.

Zhang, S., Wu, J., Wang, Y. G., Jeng, D. S., & Li, G. (2022). A physics-informed statistical learning framework for forecasting local suspended sediment concentrations in marine environment. *Water Research, 218*, 118518.

Zhang, S., Zhao, Z., Nielsen, P., Wu, J., Jia, Y., Li, G., & Li, S. (2023). Subaqueous silt ripples measured by an echo sounder: Implications for bed roughness, bed shear stress and erosion threshold. *Journal of Hydrology, 626*, 130354.

Zhang, S., Zhao, Z., Wu, J., Perrochet, P., Wang, Y. G., Li, G., & Li, S. (2024). Optimization of suspended particulate transport parameters from measured concentration profiles with a new analytical model. *Water Research, 254*, 121407.

Zhu, C., van Maren, D. S., Guo, L., Lin, J., He, Q., & Wang, Z. B. (2021). Effects of sediment-induced density gradients on the estuarine turbidity maximum in the Yangtze Estuary. *Journal of Geophysical Research: Oceans, 126*(5), e2020JC016927.

Zhu, C., van Maren, D. S., Guo, L., Lin, J., He, Q., & Wang, Z. B. (2022). Feedback effects of sediment suspensions on transport mechanisms in an estuarine turbidity maximum. *Journal of Geophysical Research: Oceans, 127*(6), e2021JC018029.

Please cite this article as: Do, T.-K.-A et al., Three-dimensional numerical modeling of sediment transport in a highly turbid estuary with pronounced seasonal variations, International Journal of Sediment Research, https://doi.org/10.1016/j.ijsrc.2024.12.003